

Cite this: *J. Mater. Chem. C*, 2023,  
11, 8129

## Thermal quenching of lanthanide luminescence via charge transfer states in inorganic materials

Pieter Dorenbos 

There are various routes of luminescence quenching such as multi-phonon relaxation from excited states to lower energy states, energy migration to killer sites, and radiation less relaxation to the ground state via the crossing point in a configurational coordinate diagram. In this work, we will consider and review quenching of lanthanide luminescence by means of charge carrier transfer to the valence band or the conduction band of the host compound. We will focus on  $4f^n-4f^n$  emission quenching due to thermally activated electron transfer from the  $\text{Pr}^{3+} \ ^3\text{P}_0$  level and the  $\text{Tb}^{3+} \ ^5\text{D}_4$  level to the conduction band, and due to thermally activated hole transfer from the  $\text{Eu}^{3+} \ ^5\text{D}_0$  level to the valence band. In addition, we will consider the quenching of the  $4f^{n-1}5d-4f^n$  emission of  $\text{Eu}^{2+}$  and  $\text{Ce}^{3+}$  which often (if not always) proceeds by electron transfer to the conduction band. Since all the above quenching routes involve reduction or oxidation of lanthanides, the location of the lanthanide charge transition levels with respect to the host bands is crucial. In other words, we need to know the location of the ground and excited states in the band gap or equivalently the vacuum referred binding energies (VRBE) in the lanthanide states as can be established using the (refined) chemical shift model. A clear correlation between the temperature  $T_{50}$  at which luminescence intensity or luminescence decay time has dropped by 50% and thermal quenching activation energies  $\Delta E$  derived from VRBE schemes will be demonstrated. Since  $T_{50}$  typically changes 400–800 K with a 1 eV change in  $\Delta E$ , and since VRBE energies may contain 0.3–0.5 eV error, it will be clear that the accurate prediction of quenching temperatures from the VRBE data is not yet feasible. Nevertheless, one may derive trends and provide guidelines on how to improve the thermal stability of luminescence.

Received 19th October 2022,  
Accepted 1st December 2022

DOI: 10.1039/d2tc04439k

rsc.li/materials-c

### Anniversary statement

Ten years ago, the *J. Mater. Chem. C* was a 'new kid on the block' in our field of luminescence phosphors. It has evolved quite rapidly into a high impact factor journal publishing manuscripts related to luminescence materials and their application in devices. We together with collaborating groups have almost yearly published manuscripts in *JMCC* on topics such as thermal quenching in Ce doped garnets, persistent luminescence, carrier dynamics and trapping in phosphors, computational studies on the spectroscopy of lanthanides, and conduction and valence band engineering of phosphor properties. The high impact factor is reflected in the frequency of citations to our work.

## 1 Introduction and theory

The thermal quenching of luminescence is an important phosphor characteristic for many different applications. For application at room temperature, the onset for thermal quenching should obviously be well above 300 K. Luminescent phosphors in modern day light emitting diode (LED) lighting like  $\text{Ce}^{3+}$  doped garnet  $\text{Y}_3\text{Al}_5\text{O}_{12}$  typically operate at temperatures around 100 C,<sup>1</sup> and phosphors should not start to quench then. High

power white light emitting (WLED) phosphors require thermal stability up to at least 200 C (475 K).<sup>1,2</sup> The thermal quenching of emission intensity or emission decay time is also used in thermometry.<sup>3–5</sup> Thermal barrier coating phosphors (TBCs) are used to sense the temperature in turbine engines up to temperatures as high as 1200 K, see, *e.g.*, ref. 6 and 7. Understanding how the quenching temperature depends on the type of the luminescence activator and the type of host compound is then important for research and development, or even for engineering of new phosphor materials towards a specific application. Luminescence intensity can be decreased by various quenching mechanisms as illustrated in Fig. 1 where a luminescence center with a ground state (g.s.) and several

Delft University of Technology, Faculty of Applied Sciences, Department of Radiation Science and Technology, Mekelweg 15, 2629 JB Delft, The Netherlands.  
E-mail: p.dorenbos@tudelft.nl; Tel: +31 15 2781336











was found which agrees well with the prediction from eqn (4) as listed in Table 1.

In this work, we added new information. We selected compounds with a relatively low  $\text{Eu}^{3+}$  concentration (about 1%). Often, the data for decay time quenching were preferred over those of intensity quenching because the latter tend to be less accurate. The results are shown in Fig. 4 and the data and references are found in Table 2. We also added information on  $E^{\text{ex}}$  and the  $U$ -values from which the data on  $E_{\text{V}}$  and  $E_{\text{C}}$  are obtained using the refined chemical shift model. The typical error bars are  $\pm 0.12$  eV in the CT-energy and  $\pm 50$  K in the  $T_{10}$  value.  $\Delta E$  on the horizontal axis was obtained by

$$\Delta E = E^{\text{CT}} - E(^5\text{D}_0) - 5 \times 10^{-5} T_{10} E^{\text{ex}} \quad (5)$$

where  $5 \times 10^{-5} T_{10} E^{\text{ex}}$  is the estimated lowering of the bandgap at a temperature  $T_{10}$  where we assumed that the amount of lowering scales with  $E^{\text{ex}}$ . This is motivated as follows. The VRBE of cation electrons lowers (becomes more negative) when neighboring anions move further away; this is simply a matter of less Coulombic repulsion from the negatively charged anions. The VRBE of anion electrons raises (becomes less negative) when neighboring cations move further away; this is a matter of decreased Coulombic attraction from the positively charged cations. As a result, the cation related CB-bottom moves down and the anion related VB-top moves up causing the bandgap to decrease. For  $\text{Eu}^{2+}$ , being a cation, we will assume that its VRBE lowers with the same pace as the CB-bottom. Since the VB-top moves upwards,  $\Delta E$  will decrease with the same amount as the bandgap lowering.

There are few outliers notably  $\text{ScBO}_3$ ,  $\text{ScPO}_4$  and  $\text{YVO}_4$  as shown in Fig. 4. Disregarding these, a linear least square fit through the data yields the dashed line with a slope of  $421 \text{ K eV}^{-1}$  which agrees very good with a predicted value of  $435 \text{ K eV}^{-1}$  as shown in Table 1. The compound to compound variation in decay time, in maximum phonon frequencies, and

**Table 2** Data on  $T_{10}$  values for the  $\text{Eu}^{3+} ^5\text{D}_0$  emission and the quenching energy barriers  $\Delta E$  derived from  $E^{\text{CT}}$  and  $E^{\text{ex}}$  energies. The parameters used for the VRBE-diagram construction are provided. All energies are in eV

A	$U$	$E^{\text{CT}}$	$E_{\text{V}}$	$E^{\text{ex}}$	$E_{\text{C}}$	$\Delta E$	$T_{10}$	Ref.
LaOCl	6.65	4.20	-8.10	6.45	-1.32	1.85	550	19
YOCl	6.65	4.54	-8.44	7.10	-0.94	2.14	630	20
YOBr	6.57	4.32	-8.18	6.50	-1.34	1.93	650	20
LaPO <sub>4</sub>	7.18	4.84	-9.00	8.10	-0.38	2.37	720	7
LuPO <sub>4</sub>	7.08	5.74	-9.85	8.70	-0.55	3.09	1085	7,21
ScPO <sub>4</sub>	7.02	5.95	-10.0	7.40	-2.19	3.42	950	7,22
LaBO <sub>3</sub>	6.93	4.51	-8.54	7.05	-1.10	2.10	650	23,24
ScBO <sub>3</sub>	6.86	5.44	-9.44	7.10	-1.94	3.01	700	24
Ca <sub>2</sub> Gd <sub>6</sub> (SiO <sub>4</sub> ) <sub>6</sub> O <sub>2</sub>	6.80	4.59	-8.56	7.00	-1.17	2.20	600	7
X <sub>2</sub> -Y <sub>2</sub> SiO <sub>5</sub> :(Ce1)	6.86	4.80	-8.80	6.82	-1.61	2.32	890	7,25
LaAlO <sub>3</sub>	6.76	3.91	-7.86	6.10	-1.47	1.58	500	26
GdAlO <sub>3</sub>	6.75	4.75	-8.70	7.36	-0.90	2.31	700	4
Y <sub>3</sub> Al <sub>5</sub> O <sub>12</sub>	6.77	5.23	-9.19	7.10	-1.69	2.69	1020	7
Li <sub>2</sub> Mg <sub>2</sub> (WO <sub>4</sub> ) <sub>3</sub>	7.15	4.07	-8.21	4.70	-3.34	1.78	465	27
YVO <sub>4</sub>	6.80	4.10	-8.07	4.00	-3.94	1.76	800	7
MgLa <sub>2</sub> TiO <sub>6</sub>	6.68	3.88	-7.79	4.50	-3.13	1.60	410	28
Gd <sub>2</sub> Ti <sub>2</sub> O <sub>7</sub>	6.79	3.94	-7.91	4.15	-3.62	1.68	400	29
Y <sub>2</sub> Ti <sub>2</sub> O <sub>7</sub>	6.79	3.85	-7.82	4.25	-3.42	1.56	500	2
Zr <sub>0.83</sub> Y <sub>0.17</sub> O <sub>1.91</sub>	6.70	4.34	-8.26	5.40	-2.63	1.96	740	7,30
La <sub>2</sub> Zr <sub>2</sub> O <sub>7</sub>	6.66	4.43	-8.33	6.00	-2.05	2.06	620	5,31
La <sub>2</sub> Hf <sub>2</sub> O <sub>7</sub>	6.65	4.40	-8.30	6.00	-2.01	2.03	625	5,31
La <sub>2</sub> Be <sub>2</sub> O <sub>5</sub>	6.70	4.11	-8.03	6.28	-1.44	1.78	480	32
Gd <sub>2</sub> Zr <sub>2</sub> O <sub>7</sub>	6.65	4.81	-8.71	6.00	-2.42	2.41	725	6
C-Gd <sub>2</sub> O <sub>3</sub> :(S <sub>6</sub> )	6.60	4.86	-8.74	5.50	-2.99	2.47	775	33
C-Y <sub>2</sub> O <sub>3</sub> :(S <sub>6</sub> )	6.60	5.05	-8.93	6.10	-2.53	2.60	890	33,34
C-Sc <sub>2</sub> O <sub>3</sub> :(C <sub>2</sub> )	6.60	5.02	-8.90	6.30	-2.28	2.54	950	33
La <sub>2</sub> O <sub>2</sub> S	6.37	3.64	-7.41	4.75	-2.48	1.37	400	19,35
Y <sub>2</sub> O <sub>2</sub> S	6.37	3.76	-7.53	4.85	-2.49	1.47	460	19
KLuS <sub>2</sub>	6.20	3.02	-6.71	4.35	-2.21	0.81	150	36
YSiO <sub>2</sub> N	6.70	3.89	-7.81	6.10	-1.41	1.58	425	37
AlN-wurtzite	6.40	3.49	-7.27	6.20	-0.76	1.22	300	38
GaN-wurtzite	6.40	3.25	-7.03	3.48	-3.45	1.04	200	38-40

in relaxation effects, and the experimental errors in  $E^{\text{CT}}$  and  $T_{10}$  then provide the scatter of data.

Note that the fitted line does not cross the horizontal at zero energy but near 0.5 eV. We assumed that quenching occurs by the full ionization of the hole. However, this is not necessarily needed. The CT-state is a hole at the valence band that is still Coulomb bonded with the transferred electron, *i.e.*,  $\text{Eu}^{2+}$ , and radiation less recombination may start from this bonded state which will lower  $\Delta E$ . Furthermore, 0.5 eV is of the same magnitude as the energy involved in lattice relaxation and Stokes shift.<sup>15,41</sup> We therefore interpret the intercept near 0.5 eV as an effect of electron-hole bonding and lattice relaxation.

## B. Thermal quenching of the $\text{Tb}^{3+} ^5\text{D}_4$ emission

The energy gap between the emitting  $^5\text{D}_4$  level of  $\text{Tb}^{3+}$  and the next lower  $^7\text{F}_0$   $4\text{f}^8$ -level is about 1.8 eV. This is even larger than that in the case of  $\text{Eu}^{3+}$  considered above, and multi-phonon relaxation is like for  $\text{Eu}^{3+}$  not a feasible quenching mechanism. Instead, in cases where the CB-bottom is not too far above the  $^5\text{D}_4$  level, thermal quenching can proceed by electron ionization to the CB. For  $\text{YPO}_4$  in Fig. 3 with the CB-bottom at  $-0.63$  eV, the distance is 4.5 eV which is clearly too large. However, in transition metal based compounds like tantalates, tungstates, vanadates, niobates, molybdates and titanates, the CB-bottom appears at  $-3$  eV to  $-4$  eV.<sup>42</sup> The excitation spectra

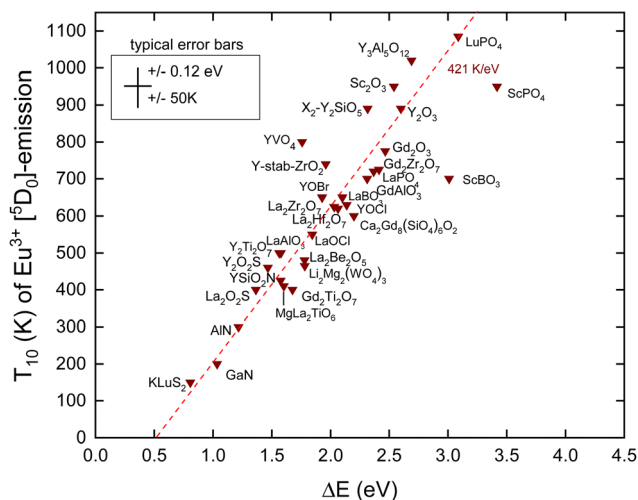


**Fig. 4** 10% Quenching temperature  $T_{10}$  for the  $\text{Eu}^{3+}$  emission from the  $^5\text{D}_0$  level against the energy difference between the  $^5\text{D}_0$  hole state and the VB-top. The fitted dashed line has a slope of  $421 \text{ K eV}^{-1}$ .



of the  $Tb^{3+}$  emission in these compounds often reveal a so-called intervalence charge transfer (IVCT) band attributed to the excitation of an electron from the  $Tb^{3+} 7F_6$  ground state<sup>43,44</sup> to the CB. Whereas the CT-band energy of  $Eu^{3+}$  provides the location of the  $Eu^{2+}$  ground state above the VB, the IVCT band provides the  $Tb^{3+}$  ground state below the CB. Therefore, the IVCT band energy determines the quenching energy barrier  $\Delta E$  and therewith the quenching temperature  $T_{50}$ . This was already demonstrated for  $Tb^{3+}$  in transition metal element based compounds in ref. 42. In ref. 14, compounds such as  $SnO_2$ ,  $Ga_2O_3$ ,  $Lu_2O_3$ , and  $GaN$  with low lying conduction bands were added to the collection.

IVCT bands are  $\approx 0.8$  eV broad and in many compounds they tend to overlap partly with the host excitation band. This introduces often larger errors in the derived value for the IVCT energy  $E^{IVCT}(Tb^{3+})$ . To improve accuracy, one may construct a VRBE diagram as shown in Fig. 3 that combines the spectroscopic data on many different lanthanides thus leading to more accurate  $\Delta E$  values. This method was followed in ref. 14 and 42 where VRBE diagrams were constructed using the 2012 chemical shift model.<sup>8</sup> We will adopt here the same method but now using the refined chemical shift model which provides few 0.1 eV different  $Tb^{4+/3+}$  CTL energies. The results are compiled in Table 3 and are shown in Fig. 5. Other than for  $Eu^{3+}$ , there is no need to correct for bandgap lowering with the increase of temperature because we assume that the  $Tb^{3+}$  levels move down with the same pace as the downward movement of the CB-bottom.

When assuming that the energy  $E^{IVCT}$  at the maximum of the IVCT band locates the  $Tb^{3+}$  ground state below the CB-bottom, one obtains for  $\Delta E$

$$\Delta E = E^{IVCT}(Tb^{3+}) - E(^5D_4) \quad (6)$$

where  $E(^5D_4) = 2.55$  eV is the energy of the  $^5D_4$  level above the ground state and the values on  $E^{IVCT}(Tb^{3+})$  can be found in ref. 62.

**Table 3**  $T_{50}$  data for emission from the  $^5D_4$  level of  $Tb^{3+}$  in compounds against the energy difference  $\Delta E$  between the  $^5D_4$  level and the CB-bottom. The parameters used for the VRBE-diagram construction are provided. All energies are in eV

A	$U$	$E^{CT}$	$E_V$	$E^{ex}$	$E_C$	$\Delta E$	$T_{50}$	Ref.
$SnO_2$	7.00	3.85	-7.92	3.59	-4.23	0.79	190	45
$CaSnO_3$	6.80	4.37	-8.34	4.93	-3.21	1.55	420	46
$\beta-Ga_2O_3$	6.90	4.28	-8.40	5.05	-3.15	1.80	385	47
$CaMoO_4$	7.00	4.40	-8.47	4.60	-3.70	1.32	450	48
$KLa(MoO_4)_2$	7.05	4.20	-8.29	4.60	-3.52	1.56	455	49
$KY(WO_4)_2$	7.15	4.60	-8.74	4.55	-4.03	1.18	410	50
$KLu(WO_4)_2$	7.15	4.55	-8.69	4.50	-4.03	1.18	325	51
$LaVO_4$	6.80	3.95	-7.92	4.25	-3.53	1.24	230	52
$GdVO_4$	6.84	4.05	-8.04	4.00	-3.91	0.90	140	53
$LuVO_4$	6.80	4.06	-8.03	3.85	-4.06	0.70	80	53
$LiNbO_3$	6.87	4.47	-8.47	4.62	-3.68	1.17	200	54,55
$CaNb_2O_6$	6.85	4.10	-8.10	4.75	-3.16	1.66	490	56
$YNbO_4$	6.84	4.60	-8.59	4.96	-3.43	1.38	455	56
$LiTaO_3$	6.65	4.54	-8.44	5.50	-2.70	1.87	585	55
$M'-YTbO_4$	6.78	5.10	-9.06	5.95	-2.83	1.91	750	57
$C-Lu_2O_3:(C_2)$	6.60	4.81	-8.69	5.90	-2.51	2.00	525	58
$Ga_{0.7}Al_{0.3}N$	6.40	3.22	-7.01	4.05	-2.83	1.44	250	59
$GaN$ -wurtzite	6.40	3.25	-7.03	3.48	-3.45	0.81	30	59-61

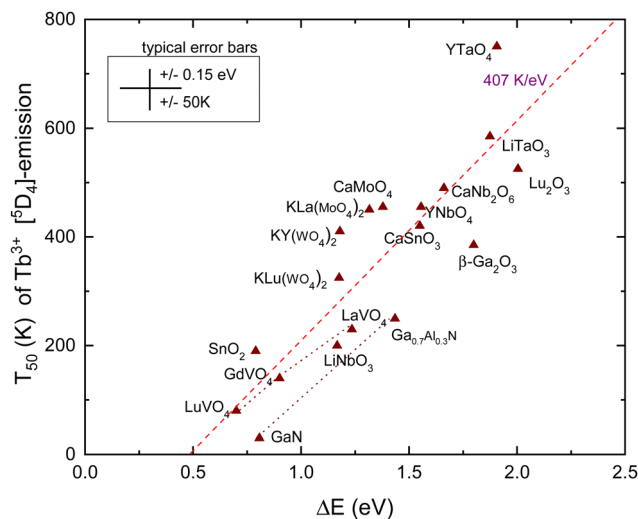


**Fig. 5**  $T_{50}$  data for emission from the  $^5D_4$  level of  $Tb^{3+}$  in compounds against the energy difference  $\Delta E$  between the  $^5D_4$  level and the CB-bottom.

When the quenching energy barrier is derived from the VRBE diagram construction one obtains for  $\Delta E$

$$\Delta E = [E^{ex} + 0.008(E^{ex})^2] - [E^{CT} - U + \Delta E(Eu, Tb) + E(^5D_4)] \quad (7)$$

where the first term between square brackets is the energy of the CB-bottom with respect to the VB-top and the second term of the  $^5D_4$  state with respect to the VB-top where  $\Delta E(Eu, Tb) \approx 3.5$  eV is the slightly compound dependent energy difference between the  $Eu^{3+}$  and  $Tb^{3+}$  ground state energies. The energy  $E^{CT}$  is not necessarily experimentally determined from the energy of the  $Eu^{3+}$  CT-band. It is often deduced from the constructed VRBE schemes that can be based, e.g., on CT-bands other than that of  $Eu^{3+}$ , experimental IVCT energies, or photoelectron spectroscopy data.

The dashed line in Fig. 5 is from a linear least squares fit through the data and has a slope of  $407 \text{ K eV}^{-1}$ . This is somewhat smaller than the value of  $475 \text{ K eV}^{-1}$  predicted in Table 1. Nevertheless, a clear correspondence between the quenching temperature and the energy at the CB-bottom is evident. The situation and figure much resemble that of hole ionization in the case of  $Eu^{3+}$  as shown in Fig. 4. The similar lifetimes of 1–2 ms for  $Eu^{3+}$  and  $Tb^{3+}$  emissions result in similar slopes in the linear fits. Also, the intersection with the horizontal axis for both dopants occurs near 0.5 eV.

Note that the  $^5D_3$  level of  $Tb^{3+}$  is located 0.7 eV above the  $^5D_4$  level and therefore located 0.7 eV closer to the CB-bottom. Since the  $^5D_3$  and  $^5D_4$  lifetimes differ not too much (factor of 2), one may expect about 350 K lower thermal stability of the  $^5D_3$  emission. Indeed, the difference amounts 375 K for  $CaMoO_4$ <sup>63</sup> and 370 K for  $CaNb_2O_6$ .<sup>56</sup> Furthermore, whenever  $T_{50}(^5D_4) < 300$  K, the emission from  $^4D_3$  is absent even down to 4 K. This can be verified with the data compiled in ref. 42.

### C. Thermal quenching of the $Pr^{3+} 3P_0$ emission

The  $Pr^{4+/3+}$  CTL is near the same energy as that for  $Tb^{4+/3+}$ . Also, the emitting  $^3P_0$  level of  $Pr^{3+}$  is near the same VRBE as that for



the  $^5D_4$  level of  $Tb^{3+}$  as can be seen in the scheme for  $YPO_4$  in Fig. 3. This means that like for  $Tb^{3+}$  thermal quenching may proceed by electron ionization to the CB in compounds with the low lying CB-bottom. Other than  $Tb^{3+}$  and  $Eu^{3+}$ , the next lower excited state ( $^1D_2$ ) is only at  $\Delta E_{mp} = 0.5$  eV lower energy. At a sufficiently high temperature, the multi-phonon relaxation to  $^1D_2$  then becomes also a possible quenching route. The radiative lifetime of the  $^3P_0$  state is usually between 10 and 50  $\mu s$  and is therefore shorter than those of  $Eu^{3+}$  and  $Tb^{3+}$ . This translates to a steeper  $T_{50}/\Delta E = 560$  K  $eV^{-1}$  slope as shown in Table 1. In ref. 42, a relationship between  $T_{50}$  of the  $^3P_0$  emission and the energy of the IVCT band, or equivalently the energy distance from the CB-bottom, was already demonstrated. Since then, more data have become available. Here, we have re-analyzed everything with the refined chemical shift model. The results are shown in Fig. 6 and compiled in Table 4.

For the quenching energy barrier, we used the same method as for  $Tb^{3+}$ . When assuming that the energy  $E^{IVCT}(Pr^{3+})$  at the maximum of the IVCT band locates the  $Pr^{3+}$  ground state below the CB-bottom one obtains for  $\Delta E$

$$\Delta E = E^{IVCT}(Pr^{3+}) - E(^3P_0) \quad (8)$$

where  $E(^3P_0) = 2.55$  eV is the energy of the  $^3P_0$  level above the ground state and the values on  $E^{IVCT}(Pr^{3+})$  can be found in ref. 62.

When the quenching energy barrier is derived from the VRBE construction one obtains for  $\Delta E$

$$\Delta E = [E^{ex} + 0.008(E^{ex})^2] - [E^{CT} - U + \Delta E(Eu, Pr) + E(^3P_0)] \quad (9)$$

where  $\Delta E(Eu, Pr) \approx 3.49$  eV is the energy difference between the  $Eu^{3+}$  and  $Pr^{3+}$  ground state energies.

The dashed line drawn through the data has a slope of 560 K  $eV^{-1}$  as predicted from Table 1. It crosses the horizontal axis near 0.3 eV which compares with that for  $Tb^{3+}$  and  $Eu^{3+}$

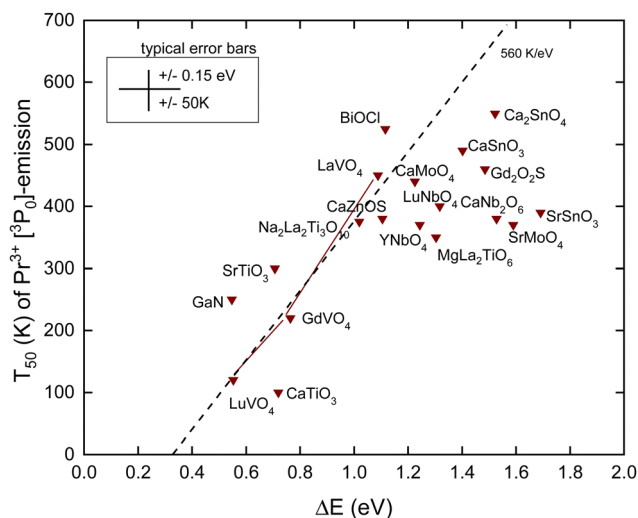


Fig. 6  $T_{50}$  data for the emission from the  $^3P_0$  level of  $Pr^{3+}$  in compounds against the energy difference  $\Delta E$  between the  $^3P_0$  level and the conduction band bottom.

Table 4  $T_{50}$  data for emission from the  $^3P_0$  level of  $Pr^{3+}$  in compounds against the energy difference between the  $^3P_0$  level and the CB-bottom. The parameters used for the VRBE-diagram construction are provided. All energies are in eV

A	U	$E^{CT}$	$E_V$	$E^{ex}$	$E_C$	$\Delta E$	$T_{50}$	Ref.
BiOCl	6.70	3.55	-7.47	4.00	-3.34	1.12	525	64
SrSnO <sub>3</sub>	6.96	4.00	-8.05	4.70	-3.17	1.69	390	65
CaSnO <sub>3</sub>	6.80	4.37	-8.34	4.93	-3.21	1.40	490	65
Ca <sub>2</sub> SnO <sub>4</sub>	6.85	4.43	-8.42	5.05	-3.17	1.52	550	65
SrMoO <sub>4</sub>	7.05	4.25	-8.34	4.75	-3.41	1.59	≈ 370	66
CaMoO <sub>4</sub>	7.00	4.40	-8.47	4.60	-3.70	1.23	440	67
LaVO <sub>4</sub>	6.80	3.95	-7.92	4.25	-3.53	1.09	450	44
GdVO <sub>4</sub>	6.84	4.05	-8.04	4.00	-3.91	0.76	220	53
LuVO <sub>4</sub>	6.80	4.06	-8.03	3.85	-4.06	0.55	120	53
CaNb <sub>2</sub> O <sub>6</sub>	6.85	4.10	-8.10	4.75	-3.16	1.53	380	56
YNbO <sub>4</sub>	6.84	4.60	-8.59	4.96	-3.43	1.24	370	56
LuNbO <sub>4</sub>	6.85	4.58	-8.58	5.00	-3.38	1.32	400	68
SrTiO <sub>3</sub>	6.75	3.44	-7.39	3.46	-3.83	0.71	≈ 300	69,70
CaTiO <sub>3</sub>	6.75	3.84	-7.79	3.85	-3.82	0.72	≈ 100	69,70
Na <sub>2</sub> La <sub>2</sub> Ti <sub>3</sub> O <sub>10</sub>	6.75	3.70	-7.65	4.00	-3.52	1.02	375	71
MgLa <sub>2</sub> TiO <sub>6</sub>	6.68	3.88	-7.79	4.50	-3.13	1.30	350	72
CaZnOS	6.35	3.73	-7.49	4.51	-2.82	1.11	380	73
Gd <sub>2</sub> O <sub>2</sub> S	6.37	3.72	-7.49	4.83	-2.47	1.49	460	74
GaN-wurtzite	6.40	3.25	-7.03	3.48	-3.45	0.55	250	75,76

where the crossing was near 0.5 eV. The data seem initially to follow this slope, but when  $T_{50}$  approaches 400 K many data points start to level off. The mentioned multi-phonon relaxation to the  $^1D_0$  level may be responsible for this. A detailed analysis for each compound would be required to resolve this further. It is interesting to compare the results for the sequence of compounds  $LaVO_4$ ,  $GdVO_4$ , and  $LuVO_4$  where the bottom of the CB-band is formed by the lowest 3d-orbitals of  $V^{4+}$ .<sup>42</sup> In this sequence, this CB-bottom lowers by about 0.5 eV, see column 6 in Tables 3 and 4. For both the  $Tb^{3+}$   $^5D_4$  emission and the  $Pr^{3+}$   $^3P_0$  emission, this leads to increasingly lower  $T_{50}$  as seen in Fig. 5 and 6.

The  $^1G_4$  level of  $Pr^{3+}$  is  $\Delta E_{mp} = 0.86$  eV below the  $^1D_2$  level which makes multi-phonon relaxation from  $^1D_2$  less probable than that from the  $^3P_0$  level. The quenching of the  $^1D_2$  emission may again proceed *via* the CB. Although the lifetime of the  $^1D_2$  level is about 10 times longer than that of  $^3P_0$  its 0.5 eV further distance below the CB is more important leading to the significantly higher thermal stability of the  $^1D_2$  emission. The difference in  $T_{50}$  for  $CaNb_2O_6$ ,<sup>56</sup>  $LuNbO_4$ ,<sup>68</sup> and  $MgLa_2TiO_6$ <sup>72</sup> appears about 200 K in line with the expectation.

#### D. Thermal quenching of the $Eu^{2+}$ $4f^6$ $5d-4f^7$ emission

Techniques such as photoconductivity, excited state absorption, delayed fluorescence, and thermoluminescence charging studies have evidenced that the quenching of the  $Eu^{2+}$  emission proceeds often, if not always, by means of the thermal ionization of the 5d electron to the CB. The consistency between quenching *via* the CB and  $Eu^{2+}$  level locations with respect to the CB-bottom was demonstrated in ref. 77. The same was concluded from first principles studies on fifteen representative  $Eu^{2+}$ -doped phosphors by Jia *et al.*<sup>78</sup>

The nature of the 5d-4f emission is much different from that of the  $4f^n-4f^n$  emission. The transition is dipole allowed



**Table 5**  $T_{50}$  data for the  $\text{Eu}^{2+}$  5d–4f emission in compounds (A) against the energy difference between the lowest energy of the relaxed 4f<sup>6</sup> 5d level and the CB-bottom. The parameters used for the VRBE-diagram construction are provided. All energies are in eV

A	$U$	$E^{\text{CT}}$	$E_{\text{V}}$	$E^{\text{ex}}$	$E_{\text{C}}$	$E_{\text{fd}}$	$\Delta S$	$\Delta E$	$T_{50}$	Ref.
RbCl <sup>a</sup>	6.70	4.20	−8.12	7.54	−0.13	3.19	0.21	1.01	670	83
KCl <sup>a</sup>	6.70	4.23	−8.15	7.79	0.12	3.10	0.17	1.16	770	83
NaCl <sup>a</sup>	6.70	4.48	−8.40	7.96	0.06	3.02	0.12	1.15	850	83
RbBr <sup>a</sup>	6.60	3.10	−6.98	6.64	0.02	3.16	0.17	1.02	690	83
KBr <sup>a</sup>	6.60	3.53	−7.41	6.80	−0.24	3.14	0.22	1.14	717	83
NaBr <sup>a</sup>	6.60	3.40	−7.28	6.75	−0.16	3.02	0.13	0.96	740	83
CsI <sup>a</sup>	6.25	2.60	−6.31	5.80	−0.24	2.97	0.19	0.50	220	84
KI <sup>a</sup>	6.25	3.00	−6.71	5.88	−0.56	3.07	0.20	0.99	450	85
Ba <sub>5</sub> (PO <sub>4</sub> ) <sub>3</sub> Cl	6.89	4.40	−8.41	7.30	−0.69	3.05	0.20	0.37	510	86,87
Sr <sub>5</sub> (PO <sub>4</sub> ) <sub>3</sub> Cl	6.90	4.66	−8.68	7.50	−0.73	2.92	0.15	0.45	460	88
Ca <sub>5</sub> (PO <sub>4</sub> ) <sub>3</sub> Cl	6.88	5.04	−9.05	7.70	−0.88	2.97	0.24	0.28	480	87,89
Ca <sub>2</sub> BO <sub>3</sub> Cl	6.77	4.49	−8.45	7.15	−0.89	2.68	0.43	0.60	450	90
Ca <sub>3</sub> Mg(SiO <sub>4</sub> ) <sub>4</sub> Cl <sub>2</sub>	6.60	4.47	−8.35	6.95	−1.01	2.61	0.16	0.34	425	91
α-Sr <sub>2</sub> P <sub>2</sub> O <sub>7</sub>	7.13	4.68	−8.81	7.85	−0.47	3.12	0.16	0.62	470	92
LiSrPO <sub>4</sub>	7.05	4.77	−8.86	7.75	−0.63	2.95	0.20	0.61	450	93
Ca <sub>10</sub> K(PO <sub>4</sub> ) <sub>7</sub>	7.05	5.06	−9.15	8.00	−0.64	2.95	0.27	0.64	450	94
NaCaPO <sub>4</sub>	7.07	4.77	−8.87	7.75	−0.64	2.77	0.31	0.85	600	95,96
YPO <sub>4</sub>	7.09	5.65	−9.77	8.55	−0.63	2.94	0.04	0.57	230	97
LuPO <sub>4</sub>	7.08	5.74	−9.85	8.70	−0.55	2.94	0.05	0.65	230	97
BaB <sub>8</sub> O <sub>13</sub>	7.30	5.15	−9.38	8.15	−0.69	3.35	0.24	0.30	500	98,99
SrB <sub>6</sub> O <sub>10</sub>	7.31	5.49	−9.71	8.30	−0.86	3.35	0.15	0.08	300	100
Ba <sub>2</sub> Ca(BO <sub>3</sub> ) <sub>2</sub>	6.93	4.61	−8.64	6.90	−1.36	2.79	0.38	0.07	190	101
NaBa <sub>4</sub> (BO <sub>3</sub> ) <sub>3</sub>	6.84	4.58	−8.57	7.00	−1.18	2.64	0.35	0.35	280	102
NaSr <sub>4</sub> (BO <sub>3</sub> ) <sub>3</sub>	6.85	4.65	−8.64	7.20	−1.03	2.67	0.69	0.64	370	102
BaBPO <sub>5</sub>	7.24	4.81	−9.00	8.53	0.12	3.42	0.16	0.97	565	103
SrBPO <sub>5</sub>	7.22	4.96	−9.14	8.53	−0.03	3.49	0.29	0.80	450	103
α-CaAl <sub>2</sub> B <sub>2</sub> O <sub>7</sub>	7.03	4.96	−9.04	7.30	−1.32	3.06	0.18	−0.21	60	104
CaBPO <sub>5</sub>	7.22	5.06	−9.24	8.55	−0.11	3.31	0.23	0.88	265	103
α-SrSiO <sub>3</sub>	6.63	5.04	−8.93	7.70	−0.76	3.02	0.21	0.21	130	105
CaMgSi <sub>2</sub> O <sub>6</sub>	7.03	5.10	−9.18	7.95	−0.73	2.97	0.20	0.49	390	106
Ba <sub>2</sub> MgSi <sub>2</sub> O <sub>7</sub>	6.95	4.34	−8.38	7.00	−0.99	2.84	0.37	0.40	460	107,108
Sr <sub>2</sub> MgSi <sub>2</sub> O <sub>7</sub>	7.03	4.75	−8.83	7.29	−1.12	2.82	0.19	0.24	250	109,110
BaCa <sub>2</sub> Mg(SiO <sub>4</sub> ) <sub>2</sub>	6.90	4.20	−8.22	7.85	0.12	3.31	0.42	1.05	530	111,112
Ba <sub>2</sub> SiO <sub>4</sub>	6.87	4.35	−8.36	7.05	−0.91	2.70	0.24	0.52	420	113–115
Sr <sub>3</sub> Mg(SiO <sub>4</sub> ) <sub>2</sub>	6.91	4.54	−8.57	7.45	−0.67	3.02	0.32	0.49	515	116
Sr <sub>2</sub> SiO <sub>4</sub>	6.81	4.64	−8.61	7.20	−1.00	3.19	0.55	0.07	425	117
Li <sub>2</sub> SrSiO <sub>4</sub>	6.91	4.81	−8.83	7.12	−1.30	2.43	0.26	0.42	525	118
CaAl <sub>2</sub> (SiO <sub>4</sub> ) <sub>2</sub>	6.95	4.44	−8.48	7.50	−0.53	3.08	0.19	0.53	480	119
Ca <sub>3</sub> Mg(SiO <sub>4</sub> ) <sub>2</sub>	6.86	4.96	−8.96	7.60	−0.90	3.02	0.41	0.28	435	116,120
β-Ca <sub>2</sub> SiO <sub>4</sub>	6.80	4.77	−8.74	7.25	−1.07	2.86	0.41	0.24	390	107
Li <sub>2</sub> CaSiO <sub>4</sub>	6.92	4.77	−8.80	7.55	−0.79	2.73	0.14	0.58	450	121
Sr <sub>3</sub> SiO <sub>5</sub>	6.74	4.07	−8.01	6.50	−1.17	2.43	0.29	0.48	485	122
BaAl <sub>2</sub> O <sub>4</sub>	6.82	4.63	−8.61	7.20	−1.00	2.92	0.44	0.29	270	123,124
Sr <sub>2</sub> Al(AlSiO <sub>7</sub> )	6.82	4.79	−8.77	7.50	−0.82	2.88	0.23	0.39	300	125
SrAl <sub>12</sub> O <sub>19</sub>	7.06	4.75	−8.85	8.00	−0.33	3.54	0.43	0.43	375	126
SrAl <sub>4</sub> O <sub>7</sub>	6.89	5.02	−9.03	8.00	−0.52	3.10	0.47	0.63	260	126
SrAl <sub>2</sub> O <sub>4</sub> :(site 2)	6.80	4.55	−8.52	6.85	−1.30	3.06	0.28	−0.25	210	127,128
SrAl <sub>2</sub> O <sub>4</sub> :(site 3)	6.80	4.19	−8.16	6.85	−0.94	2.76	0.37	0.46	420	127,128
Sr <sub>4</sub> Al <sub>14</sub> O <sub>25</sub> :[HE-site]	7.10	4.77	−8.89	7.70	−0.72	3.49	0.44	0.13	400	129
Sr <sub>4</sub> Al <sub>14</sub> O <sub>25</sub> :[LE-site]	6.85	4.77	−8.77	7.70	−0.59	2.82	0.30	0.73	380	129
Ca <sub>2</sub> Al(AlSiO <sub>7</sub> )	6.83	4.98	−8.97	7.60	−0.90	2.58	0.24	0.62	340	130,131
CaAl <sub>2</sub> O <sub>4</sub>	6.80	4.73	−8.70	7.40	−0.86	3.14	0.32	0.13	320	132,133
CaO	6.31	4.88	−8.62	6.94	−1.30	1.89	0.21	0.66	250	134
Ca <sub>2</sub> SiS <sub>4</sub>	6.40	2.06	−5.84	5.00	−0.64	2.38	0.18	0.85	445	135
SrGa <sub>2</sub> S <sub>4</sub>	6.30	1.87	−5.61	4.77	−0.65	2.55	0.23	0.65	470	136,137
CaGa <sub>2</sub> S <sub>4</sub>	6.25	1.90	−5.61	4.52	−0.93	2.36	0.14	0.49	450	138
CaS	6.17	2.35	−6.03	4.70	−1.15	2.07	0.16	0.54	475	139
SrSi <sub>2</sub> O <sub>2</sub> N <sub>2</sub>	6.70	3.44	−7.36	6.35	−0.69	2.51	0.21	0.83	600	81
SrSi <sub>2</sub> AlO <sub>2</sub> N <sub>3</sub>	6.60	2.97	−6.85	5.60	−0.99	2.73	0.23	0.27	450	140
CaSi <sub>2</sub> O <sub>2</sub> N <sub>2</sub>	6.70	3.10	−7.02	6.30	−0.41	2.56	0.33	1.13	455	81
Sr <sub>2</sub> Si <sub>5</sub> N <sub>8</sub>	6.33	2.56	−6.31	5.00	−1.11	2.19	0.18	0.53	550	141
Ca <sub>2</sub> Si <sub>5</sub> N <sub>8</sub>	6.35	2.93	−6.69	5.15	−1.33	2.27	0.21	0.26	370	142
CaAlSiN <sub>3</sub>	6.22	2.64	−6.34	5.05	−1.09	2.14	0.23	0.59	640	143,144
SrMg <sub>2</sub> Al <sub>2</sub> N <sub>4</sub>	6.15	2.21	−5.88	4.10	−1.64	2.13	0.12	−0.05	290	145

<sup>a</sup> For the alkaline halides, the spectroscopic data on  $E^{\text{CT}}$  are not available. The values listed are the energy differences between the  $\text{Eu}^{3+/2+}$  CTLs and  $E_{\text{V}}$  that was obtained directly from the published photoelectron spectroscopy data.









typical for almost all compounds, and such an energy difference will imply a higher quenching temperature  $T_{50}$  for Ce. The lifetime of the  $\text{Ce}^{3+}$  5d–4f emission varies between 15 ns and 65 ns<sup>79</sup> which is about 25 times shorter than that of  $\text{Eu}^{2+}$ . This leads to the  $T_{50}/\Delta E = 850 \text{ K eV}^{-1}$  rate in Table 1.

For the study of the quenching of the  $\text{Ce}^{3+}$  5d–4f emission, the same method as for the quenching of the  $\text{Eu}^{2+}$  emission was adopted, and the used expression for  $\Delta E$  is

$$\Delta E = [E^{\text{ex}} + 0.008(E^{\text{ex}})^2] - [E^{\text{CT}} - U + \Delta E(\text{Eu, Ce}) + E_{\text{fd}}^{\text{Ce}} - 0.5\Delta S] \quad (11)$$

where  $E_{\text{fd}}$  are compiled in Table 6, and where  $\Delta E(\text{Eu, Pr}) \approx 5.52 \text{ eV}$  is the energy difference between the  $\text{Eu}^{3+}$  and  $\text{Ce}^{3+}$  ground state energies.

For  $\text{Eu}^{2+}$ , the used value for the parameter  $U$  was not of relevance for obtaining the quenching energy barrier. However, for  $\text{Ce}^{3+}$ , it will be and this adds additional uncertainty to  $\Delta E$  as derived from the VRBE scheme. The  $T_{50}$  values with references and the parameters used in the VRBE construction are compiled in Table 6.

The  $T_{50}$  and derived quenching energy barriers  $\Delta E$  are shown in Fig. 8. The data appear to scatter like those for  $\text{Eu}^{2+}$  obscuring a clear relationship between the quenching temperature  $T_{50}$  and the quenching energy barrier  $\Delta E$ . The dashed line with a slope of  $850 \text{ K eV}^{-1}$  is the predicted relationship shown in Table 1, whereas a linear fit provides only a slope of  $325 \text{ K eV}^{-1}$ . One might argue that for thermal quenching the electron need not to reach the CB-bottom but it may quench *via* CB-derived states that are still bonded to  $\text{Ce}^{4+}$ . The VRBE is then expected between  $E_X$  and  $E_C$  leading to a lowering of  $\Delta E$ . It will shift and move around the data points several 0.1 eV but the general picture remains the same.

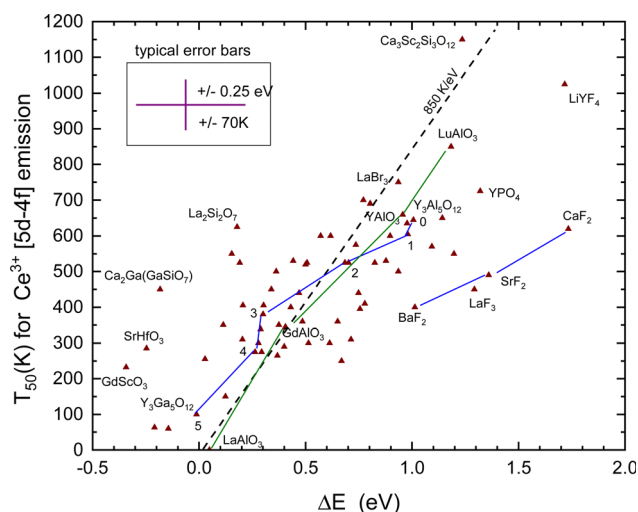


Fig. 8  $T_{50}$  quenching data of the  $\text{Ce}^{3+}$  5d–4f emission against the energy difference  $\Delta E$  between the relaxed 5d-state and the CB-bottom. The typical error bars are shown. Data points for the sequence of compounds  $\text{Y}_3\text{Al}_{5-x}\text{Ga}_x\text{O}_{12}$  and  $\text{REAlO}_3$  (RE = La, Gd, Y, Lu) are connected by straight line segments.

When we deal with a sequence of similar type of compounds systematic errors will drop out yielding better correspondence with the  $850 \text{ K eV}^{-1}$  prediction. One such sequence is  $\text{BaF}_2$ ,  $\text{SrF}_2$ , and  $\text{CaF}_2$ , where for both  $\text{Eu}^{2+}$  and  $\text{Ce}^{3+}$  the quenching temperature increases in accordance with the VRBE prediction. Furthermore,  $\text{Ce}^{3+}$  quenches at about 210 K higher temperature as  $\text{Eu}^{2+}$  also in accordance with the VRBE schemes. However, the data are located at about 0.5 eV too high  $\Delta E$  values with respect to the data on other compounds. The reason is not known but it may indicate systematic errors in the VRBE-diagram construction. Another well-studied sequence is the  $\text{Ce}^{3+}$  doped  $\text{Y}_3\text{Al}_{5-x}\text{Ga}_x\text{O}_{12}$  and  $\text{Gd}_3\text{Al}_{5-x}\text{Ga}_x\text{O}_{12}$  garnet compounds. For the sequence  $x = 0, 1, 2, 3, 4$ , and 5, the data points for  $\text{Y}_3\text{Al}_{5-x}\text{Ga}_x\text{O}_{12}$  in Fig. 8 have been connected with straight line segments. These data appear to follow the steeper slope of  $850 \text{ K eV}^{-1}$  much better. The same applies for the sequence  $\text{REAlO}_3$  (RE = La, Gd, Y, and Lu).  $\text{Ce}^{3+}$  does not emit in  $\text{LaAlO}_3$  and we assumed a  $\Delta S = 0.4 \text{ eV}$  to place the data point in Fig. 8. For  $\text{LuAlO}_3$ , we assumed  $T_{50} \approx 850 \text{ K}$  based on the work of ref. 190. Note that in the review work by Ueda and Tanabe<sup>209</sup> on  $\text{Ce}^{3+}$  doped garnet compounds the quenching data followed a slope of  $620 \text{ K eV}^{-1}$ .

Like for  $\text{Eu}^{2+}$ , there is an entire class of materials with a low lying CB-bottom and then the emitting 5d-level of  $\text{Ce}^{3+}$  is above the CB-bottom. Emission is then not observed even down to 0 K. This applies to all compounds in Tables 3 and 4.

### III. Discussion

The common aspect of the luminescence quenching of all five lanthanides considered in this work is that it proceeds *via* charge carrier transfer to the CB or the VB, and the energy difference  $\Delta E$  between the emitting level and the host band is the most relevant parameter. In this work, this value is derived from the constructed VRBE schemes. Table 1 shows the predicted relationship between  $T_{50}$  and  $\Delta E$  where a typical value for the vibrational frequency and the luminescence lifetime was assumed. A compound to compound variation in these values is unavoidable, and this will lead to the data scatter around the predicted relationships. The data for  $\text{Eu}^{3+}$  in Fig. 4 follow the predicted slope of  $435 \text{ K eV}^{-1}$  surprisingly closely. The error in  $\Delta E$  is relatively small because only the error in  $E^{\text{CT}}$  provides a dominant contribution, see eqn (5). For  $\text{Tb}^{3+}$  and  $\text{Pr}^{3+}$  in Fig. 5 and Fig. 6,  $\Delta E$  is either based on the energy at the maximum of the IVCT band, see eqn (6) and (8), which usually overlaps partly with the host excitation band preventing accurate determination. The IVCT data together with the data from other lanthanides can also be used to construct VRBE schemes. Eqn (7) and (9) can then be used to determine  $\Delta E$ . For both methods, the error in  $\Delta E$  and the scatter in data appears larger than that for  $\text{Eu}^{3+}$ ; yet, the data show consistency with the predicted slopes of  $475 \text{ K eV}^{-1}$  and  $560 \text{ K eV}^{-1}$ . For  $\text{Pr}^{3+}$ , it was suggested that above 400 K multi-phonon relaxation to the lower lying  $^1\text{D}_2$  level becomes the dominant quenching route which then causes the data to deviate from the predicted trend.









$\text{Eu}^{3+}$  charge transfer band always defines the energy difference between the  $\text{Eu}^{3+/2+}$  CTL and the VB-top may not hold for all types of compounds. One may not exclude a few 0.1 eV differences between fluorides, oxides, and sulfides leading to systematic errors in level locations and  $\Delta E$ . (3) For compounds with different sites for the activator, the same  $U$ -value is always used. A few 0.1 eV differences between different sites cannot be excluded, and there are indications of such differences. (4) The used  $U$ -values are not rigorously based on experimental or theoretical evidence and may still carry substantial errors. Despite all the above limitations, consistency between the quenching data and VRBE diagrams has been demonstrated. With a more dedicated study one might then use the quenching data as a means to further improve the method of the VRBE-diagram construction and therewith its accuracy and predictive potential.

## Conflicts of interest

There are no conflicts to declare.

## References

- H. Yamamoto, *Proc. SPIE*, 2010, **7598**, 759808.
- P. Dai, X. Zhang, M. Zhou, X. Li, J. Yang, P. Sun, C. Xu and Y. Liu, *J. Am. Ceram. Soc.*, 2012, **95**, 658.
- N. Rakov, S. A. Vieira, Q. P. S. Silva and G. S. Maciel, *Sens. Actuators, B*, 2015, **209**, 407.
- V. Lojpur, S. Culubrk, M. Medic and M. Dramicanin, *J. Lumin.*, 2016, **170**, 467.
- R. A. Hansel, S. K. Desai, S. W. Allison, A. L. Heyes and D. G. Walker, *J. Appl. Phys.*, 2010, **107**, 016101.
- M. M. Gentleman and D. R. Clarke, *Surf. Coat. Technol.*, 2005, **200**, 1264.
- M. D. Chambers and D. R. Clarke, *Annu. Rev. Mater. Res.*, 2009, **39**, 325.
- P. Dorenbos, *Phys. Rev. B: Condens. Matter Mater. Phys.*, 2012, **85**, 165107.
- P. Dorenbos, *J. Lumin.*, 2019, **214**, 116536.
- P. Dorenbos, *J. Lumin.*, 2020, **222**, 117164.
- L.-J. Lyu and D. S. Hamilton, *J. Lumin.*, 1991, **48–49**, 251.
- G. Gao, A. Turshatov, I. A. Howard, D. Busko, R. Joseph, D. Hudry and B. S. Richards, *Adv. Sustainable Syst.*, 2017, **1**, 1600033.
- P. Dorenbos, *Opt. Mater.*, 2017, **69**, 8.
- P. Dorenbos, *J. Lumin.*, 2018, **197**, 62.
- P. Dorenbos, *J. Lumin.*, 2005, **111**, 89.
- G. Blasse, *J. Chem. Phys.*, 1966, **45**, 2356.
- C. W. Struck and W. H. Fonger, *J. Lumin.*, 1970, **1–2**, 456.
- P. Dorenbos, *J. Alloys Compd.*, 2009, **488**, 568.
- W. H. Fonger and C. W. Struck, *J. Chem. Phys.*, 1970, **52**, 6364.
- Y. Kitagawa, J. Ueda, K. Arai, H. Kageyama and S. Tanabe, *J. Appl. Phys.*, 2021, **129**, 183104.
- S. W. Allison and G. T. Gillies, *Rev. Sci. Instrum.*, 1997, **68**, 2615.
- A. R. Bugos, S. W. Allison and M. R. Cates, *IEEE Proceeding Southeastcon*, 1991, 1141.
- G. Blasse and J. de Vries, *J. Electrochem. Soc.: Sol. State Sci.*, 1967, **114**, 875.
- E. P. Riedel, *J. Lumin.*, 1970, **1(2)**, 176.
- M. D. Chambers, P. A. Rousseve and D. R. Clarke, *Surf. Coat. Technol.*, 2008, **203**, 461.
- G. Blasse, A. Brill and J. A. de Poorter, *J. Chem. Phys.*, 1970, **53**, 4450.
- H. Zhu, M. Fang, Z. Huan, Y. Liu, K. Chen, X. Min, Y. Mao and M. Wang, *J. Lumin.*, 2016, **172**, 180.
- B. Bondzior, D. Stefanska, T. H. Q. Vu, N. Miniajluk-Gawel and P. J. Deren, *J. Alloys and Comp.*, 2021, **852**, 157074.
- S. J. Park, J. Y. Kim, J. H. Yim, N. Y. Kim, C. H. Lee, S. J. Yang and H. K. Yang, *J. Alloys and Comp.*, 2018, **741**, 246.
- R. J. L. Steenbakker, R. G. Wellman, J. R. Nicholls and J. P. Feist, Proc. of ASME Turbo Expo 2008: Power for Land Sea and Air GT2008, June 9–13, 2008, Berlin, Germany, GT2008-51192.
- K. S. Desai, R. A. Hansel, R. W. Pitz and D. G. Walker, 48th AIAA Aerospace Sciences Meeting Including the New Horizons Forum and Aerospace Exposition, 4–7 January 2010, Orlando, Florida, AIAA 2010-672.
- I. N. Ogorodnikov and V. A. Pustavarov, *J. Lumin.*, 2015, **162**, 50.
- G. A. West and N. S. Clements, *J. Lumin.*, 1992, **54**, 245.
- S. D. Alaruri, A. J. Brewington, M. A. Thomas and J. A. Miller, *IEEE Trans. Instrum. and Meas.*, 1993, **42**, 735.
- J. Bang, B. Abrams and P. H. Holloway, *J. Appl. Phys.*, 2003, **94**, 7091.
- V. Jary, L. Havlak, J. Barta, M. Buryi, E. M. M. Rejman, V. Laguta and M. Nikl, *Materials*, 2015, **8**, 6978.
- Y. Kitagawa, J. Ueda, M. G. Brik and S. Tanabe, *Opt. Mater.*, 2018, **83**, 111.
- A. Wakahara, *Opt. Mater.*, 2006, **28**, 731.
- T. Andreev, N. Quang Liem, Y. Hori, M. Tanaka, O. Oda, D. Le Si Dang and B. Daudin, *Phys. Rev. B: Condens. Matter Mater. Phys.*, 2006, **73**, 195203.
- C.-W. Lee, H. O. Everitt, D. S. Lee, A. J. Steckl and J. M. Zavada, *J. Appl. Phys.*, 2004, **95**, 7717.
- P. Dorenbos, *J. Phys.: Condens. Matter*, 2003, **15**, 8417.
- P. Dorenbos and E. G. Rogers, *ECS J. Solid State Sci. Technol.*, 2014, **3**, R150.
- P. Boutinaud, R. Mahiou, E. Cavalli and M. Bettinelli, *Chem. Phys. Lett.*, 2006, **418**, 185.
- P. Boutinaud, P. Putaj, R. Mahiou, E. Cavalli and A. Speghini, *Spectrosc. Lett.*, 2007, **40**, 209.
- D. F. Grabtree, *J. Phys. D: Appl. Phys.*, 1975, **8**, 2097.
- Z. Liang, J. Zhang, J. Sun, X. Li, L. Cheng, H. Zhong, S. Fu, Y. Tian and B. Chen, *Phys. B*, 2013, **412**, 36.
- Y. Tokida and S. Adachi, *ECS J. Solid State Sci. Technol.*, 2014, **3**, R100.
- E. Cavalli, P. Boutinaud, R. Mahiou, M. Bettinelli and P. Dorenbos, *Inorg. Chem.*, 2010, **49**, 4916.





- 106 F. Su, B. Lou, Y. Ou, Y. Yang, W. Zhou, C.-K. Duan and H. Liang, *J. Phys. Chem. C* **125**, 2021, 595.
- 107 G. Blasse, W. L. Wanmaker, J. W. ter Vrugt and A. Bril, *Philips Res. Rep.*, 1968, **23**, 189.
- 108 J. Yan, C. Liu, J. Vlieland, J. Zhou, P. Dorenbos, Y. Huang, Y. Tao and H. Liang, *J. Lumin.*, 2017, **183**, 97.
- 109 A. A. Setlur, A. M. Srivastava, L. Pham, M. Hannah and U. Happek, *J. Appl. Phys.*, 2008, **103**, 053513.
- 110 D. Jia, W. Jia and Y. Jia, *J. Appl. Phys.*, 2007, **101**, 023520.
- 111 D. Hou, C. Liu, X. Ding, X. Kuang, H. Liang, S. Sun, Y. Huang and Y. Tao, *J. Mater. Chem. C*, 2013, **1**, 493.
- 112 D. Hou, W. Chen, X. Ding, H. Liang, L. Zheng and J. Zhang, *ECS J. Solid State Sci. Technol.*, 2013, **2**, R79.
- 113 K. Asami, J. Ueda, K. Yasuda, K. Hongo, R. Maezono, M. G. Brik and S. Tanabe, *Opt. Mater.*, 2018, **84**, 436.
- 114 L. Lin, L. Ning, R. Zhou, C. Jiang, M. Peng, Y. Huang, J. Chen, Y. Huang, Y. Tao and H. Liang, *Inorg. Chem.*, 2018, **57**, 7090.
- 115 M. Yamaga, Y. Masui, S. Sakuta, N. Kodama and K. Kaminaga, *Phys. Rev. B: Condens. Matter Mater. Phys.*, 2005, **71**, 205102.
- 116 G. Blasse and A. Bril, *J. Chem. Phys.*, 1968, **48**, 217.
- 117 T. L. Barry, *ECS J. Solid State Sci. Technol.*, 1968, **115**, 1181.
- 118 S. S. B. Nasir, A. Tanaka, S. Yoshiara and A. Kato, *J. Lumin.*, 2019, **207**, 22.
- 119 T. J. Isaacs, *ECS J. Solid State Sci. Technol.*, 1971, **118**, 1009.
- 120 D. Stefanska and P. J. Deren, *Opt. Mater.*, 2018, **80**, 62.
- 121 J. Zhong, W. Zhao, L. Lan and J. Wang, *J. Mater. Sci.: Mater. Electron.*, 2014, **25**, 736.
- 122 Q. Shao, H. Lin, Y. Dong, Y. Fu, C. Liang, J. He and J. Jiang, *J. Solid State Chem.*, 2015, **225**, 72.
- 123 H. Aizawa, S. Komuro, T. Katsumata, S. Sato and T. Morikawa, *Thin Solid Films*, 2006, **496**, 179.
- 124 S. H. M. Poort, W. P. Blokpoel and G. Blasse, *Chem. Mater.*, 1995, **7**, 1547.
- 125 F.-C. Lu, L.-J. Bai, W. Dang, Z.-P. Yang and P. Lin, *ECS J. Solid State Sci. Technol.*, 2015, **4**, R27.
- 126 D. Dutczak, T. Justel, C. Ronda and A. Meijerink, *Phys. Chem. Chem. Phys.*, 2015, **17**, 15236.
- 127 J. Botterman, J. J. Joos and P. F. Smet, *Phys. Rev. B: Condens. Matter Mater. Phys.*, 2014, **90**, 085147.
- 128 J. Bierwagen, S. Yoon, N. Gartmann, B. Walfort and H. Hagemann, *Opt. Mater. Express*, 2016, **6**, 793.
- 129 D. Dutczak, C. Ronda, T. Justel and A. Meijerink, *J. Phys. Chem. A*, 2014, **118**, 1617.
- 130 Y. Luo and Z. Xia, *Opt. Mater.*, 2014, **36**, 1874.
- 131 T. Hu, Y. Gao, M. Molochev, Z. Xia and Q. Zhang, *Sci. China. Mater.*, 2019, **62**, 1807.
- 132 G. Blasse and A. Bril, *Philips Res. Rep.*, 1968, **23**, 201.
- 133 C. E. Tyner and H. G. Drickamer, *J. Chem. Phys.*, 1977, **67**, 4116.
- 134 S. H. M. Poort, A. Meyerink and G. Blasse, *J. Phys. Chem. Sol.*, 1997, **58**, 1451.
- 135 P. F. Smet, N. Avci and D. Poelman, *J. Electrochem. Soc.*, 2009, **156**, H243.
- 136 C. Chartier, C. Barthou, P. Benalloul and J. M. Frigerio, *J. Lumin.*, 2005, **111**, 147.
- 137 J. J. Joos, K. W. Meert, A. B. Parmentier, D. Poelman and P. F. Smet, *Opt. Mater.*, 2012, **34**, 1902.
- 138 P. Benalloul, C. Barthou, C. Fouassier, A. N. Georgobiani, L. S. Lepnev, Y. N. Emirov, A. N. Grutzintsev, B. G. Tagiev, O. B. Tagiev and R. B. Jabbarov, *J. Electrochem. Soc.*, 2003, **150**, G62.
- 139 M. Ando and Y. A. Ono, *J. Cryst. Growth*, 1992, **117**, 969.
- 140 V. Bachmann, A. Meijerink and C. Ronda, *J. Lumin.*, 2009, **129**, 1341.
- 141 R.-J. Xie, N. Hirotsaki, N. Kimura, K. Sakuma and M. Mitomo, *Appl. Phys. Lett.*, 2007, **90**, 191101.
- 142 J. Li, B. Lei, J. Qin, Y. Liu and X. Liu, *J. Am. Ceram. Soc.*, 2013, **96**, 873.
- 143 J. Ueda, S. Tanabe, K. Takahashi, T. Takeda and N. Hirotsaki, *Bull. Chem. Soc. Jpn.*, 2018, **91**, 173.
- 144 J. Tian, W. Zhuang, R. Liu, L. Wang, Y. Liu, C. Yan, G. Chen, H. Xu, M. Chen, Z. Jiang and X. Zhang, *J. Am. Ceram. Soc.*, 2019, **102**, 7336.
- 145 P. Pust, C. Hecht, V. Weiler, A. Locher, D. Zitnanska, S. Harm, D. Weichert, P. J. Schmidt and W. Schnick, *Chem. Mater.*, 2014, **26**, 6113.
- 146 R. Shendrik and E. Radzhabov, *IEEE Trans. Nucl. Sci.*, 2010, **57**, 1295.
- 147 P. Dorenbos, R. Visser, C. W. E. van Eijk, R. W. Hollander and H. W. den Hartog, *Nucl. Instrum. Methods*, 1991, **A310**, 236.
- 148 R. C. Tailor, O. H. Nestor and B. Utts, *IEEE TNS-33*, 1986, 243.
- 149 G. Bizarri, J. T. M. de Haas, P. Dorenbos and C. W. E. van Eijk, *Phys. Status Solidi A*, 2006, **203**, R41.
- 150 A. M. Srivastava, S. J. Camardello, H. A. Comanzo, M. Aycibin and U. Happek, *Opt. Mater.*, 2010, **32**, 936.
- 151 X. Zhang, B. Park, N. Choi, J. Kim, G. C. Kim and J. H. Yoo, *Mater. Lett.*, 2009, **63**, 700.
- 152 Z. Fu-Tan, C. Li-Yun and X. Xu-Rong, *ECS J. Solid State Sci. Technol.*, 1987, **134**, 3186.
- 153 D. M. de Leeuw, C. A. H. A. Mutsaers, H. Mulder and D. B. M. Klaasen, *ECS J. Solid State Sci. Technol.*, 1988, **135**, 1009.
- 154 P. Dorenbos, unpublished data.
- 155 T. Shalapska, G. Stryganyuka, D. Trotsch, T. Demkiv, A. Gektin, A. Voloshinovskii and P. Dorenbos, *J. Lumin.*, 2010, **130**, 1941.
- 156 T. Justel, P. Huppertz, W. Mayr and D. U. Wiechert, *J. Lumin.*, 2004, **106**, 225.
- 157 C.-H. Huang, T.-M. Chen and B.-M. Cheng, *Inorg. Chem.*, 2011, **50**, 6552.
- 158 H. Lin, H. Liang, Z. Tian, B. Han, J. Wang and Q. Su, *J. Phys. D: Appl. Phys.*, 2009, **42**, 165409.
- 159 Y. Yang, B. Lou, Y. Ou, F. Su, C.-G. Ma, C.-K. Duan, P. Dorenbos and H. Liang, *Inorg. Chem.*, 2022, **61**, 7654.
- 160 J. F. Chen, Y. Li, G.-L. Song, D.-M. Yao, L.-Y. Yuan, X.-J. Qi and S.-H. Wang, *J. Inorg. Mater.*, 2007, **22**(1), 25.
- 161 I. N. Ogorodnikov, N. E. Poryvai, I. N. Sedunova, A. V. Tolmachev and R. P. Yavetskiy, *Opt. Spectrosc.*, 2011, **110**, 266.





